Imaging skins: stretchable and conformable on-organ beta particle detectors for radioguided surgery

IOP Publishing Prog. Biomed. Eng. 5 (2023) 033001 https://doi.org/10.1088/2516-1091/acdc70

Progress in Biomedical Engineering

OPEN ACCESS

RECEIVED
18 October 2022

REVISED
5 May 2023

ACCEPTED FOR PUBLICATION
7 June 2023

PUBLISHED
6 July 2023

PERSPECTIVE

Imaging skins: stretchable and conformable on-organ beta particle detectors for radioguided surgery

S Dietsch[1,*], L Lindenroth[2], A Stilli[1,*] and D Stoyanov[1]

[1] Wellcome/EPSRC Centre for Interventional and Surgical Sciences, University College London, London W1W 7EJ, United Kingdom
[2] Department of Surgical & Interventional Engineering, School of Biomedical Engineering and Imaging Sciences, King's College London, London SE1 7EU, United Kingdom
[*] Authors to whom any correspondence should be addressed.

E-mail: solene.dietsch.20@ucl.ac.uk and a.stilli@ucl.ac.uk

Keywords: radioguided surgery, stretchable scintillator, radioluminescence imaging, beta-particles, nuclear imaging, minimally invasive procedure, surgical robotics

Abstract

While radioguided surgery (RGS) traditionally relied on detecting gamma rays, direct detection of beta particles could facilitate the detection of tumour margins intraoperatively by reducing radiation noise emanating from distant organs, thereby improving the signal-to-noise ratio of the imaging technique. In addition, most existing beta detectors do not offer surface sensing or imaging capabilities. Therefore, we explore the concept of a stretchable scintillator to detect beta-particles emitting radiotracers that would be directly deployed on the targeted organ. Such detectors, which we refer to as *imaging skins*, would work as indirect radiation detectors made of light-emitting agents and biocompatible stretchable material. Our vision is to detect scintillation using standard endoscopes routinely employed in minimally invasive surgery. Moreover, surgical robotic systems would ideally be used to apply the imaging skins, allowing for precise control of each component, thereby improving positioning and task repeatability. While still in the exploratory stages, this innovative approach has the potential to improve the detection of tumour margins during RGS by enabling real-time imaging, ultimately improving surgical outcomes.

1. Introduction

In 2023 cancer remains the leading cause of death worldwide [1]. By 2030, it is estimated that every year 45 million patients will require tumour removal surgery [1]. During the cancer-removal surgery, clinicians aim to ensure a negative surgical margin, meaning excising malignant tissue with an additional thin layer of healthy tissues, as illustrated in figure 1 and detailed in [2, 3]. Nonetheless, approximately 10% of surgeries result in a positive surgical margin (PSM) [4], which ultimately results in additional costs for the healthcare system due to the need for further treatment, raising anxiety levels in patients already distressed while also increasing the risks of postoperative complications [4, 5].

Multiple strategies are available to surgeons to locate the tumours and safely remove them. Usually, this process relies on preoperative medical imaging—CT, MRI, ultrasound (US)—to plan the surgery [3]. The surgical site can be marked with physical markers such as hook wires, micro coils or fluorescent dyes to enhance the visualisation of the cancerous tissues for the surgeons and any other clinician involved in the procedure. Finally, the surgeon can operate relying on another imaging technique to visualise the structures intraoperatively.

The field of intraoperative imaging, which helps clinicians to make surgical decisions in real-time, is continuously evolving. While some research groups focused on improving conventional techniques—such as radiography or US—a plethora of new intraoperative imaging techniques have emerged. Among them are surgical spectral imaging [6], fluorescence-guided surgery [7] and opto-acoustic imaging [3]. To produce a systematic review of the medical intraoperative imaging techniques available is not within the scope of this article, and more in-depth focused reviews can be found in [2, 8–11]. However, it is worth noting that none

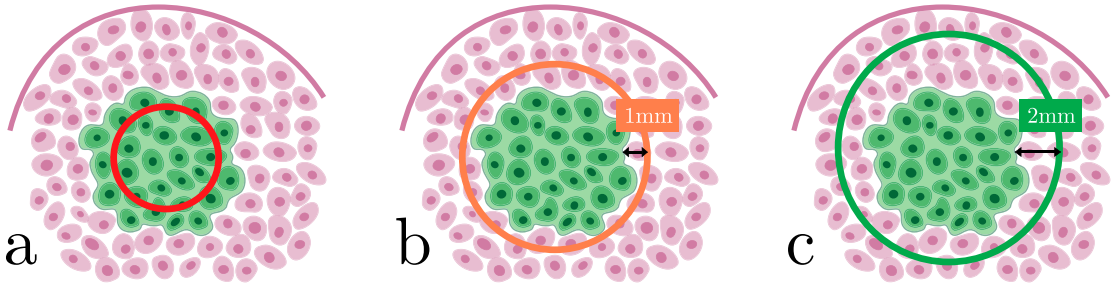

Figure 1. Schematics illustrating the concept of tumour margins in the context of breast-conserving surgery (BCS). (a) Positive surgical margin (PSM). Cancer cells are present at the edge of the excised tissue. (b) Unclear or close margin. No ink on tumour: there was no evidence of cancer cells after microscopic examination. However, the margins are not wide enough compared to BCS guidelines. (c) Negative surgical margin corresponding to BCS guideline. No cancer cells are at the outer-inked edge of the tissue.

of these techniques demonstrated results that would allow establishing a standard of care in the field [10]. Therefore, there is still a need to develop new imaging modalities to improve intraoperative tumour margin detection.

In minimally invasive surgery (MIS), the challenge deepens since access through the incision port limits visual inspection and restricts direct finger palpation and indirect palpation through a medical instrument. Besides, these methods are rarely sufficient to assess the location of the resection margins or they are still at the experimental stage [12, 13].

Radioguided surgery (RGS) is one of the oldest intraoperative imaging approaches. RGS refers to imaging techniques involving the detection of radioactively labelled tumours intra-operatively [14]. Before the surgery, the patient is injected with a radiopharmaceutical designed to accumulate in the cancerous tissues. During the surgery, the clinician operates a radiation detection probe or camera to locate the radioactive regions within the body. Then, the surgeon uses this information to excise the diseased tissues [15].

Selverstone pioneered this technique in 1949 using a β_- emitting tracer—a radioactive isotope of phosphorus, ^{32}P—to intraoperatively locate tumour residual following brain tumour excision [16]. Subsequently, most radiation probes have been tuned to detect γ radiation. Specifically, the radiopharmaceuticals were designed for the development of preoperative PET and SPECT scanners [17]. Since γ-rays are uncharged particles, they are penetrating and can only be stopped by high atomic number materials such as lead. Therefore, the radiation detector can be placed away from the source, offering more flexibility.

In contrast, beta particles—positrons (β_+) or electrons (β_-)—can only travel a few millimetres in water and tissues. What seemed to be a limitation, is now becoming a windfall with the continuous improvement of radiation detectors. Indeed, detecting β particles instead of γ would improve the detection resolution by catching the radiation closer to its source. Moreover, it removes the background noise induced by any radiation emitted from distal parts of the body, while reducing the inherent radiation exposure to the medical team [15, 18].

This intraoperative technique historically lacked crucial imaging feedback as it relied on an audible or a visible rate meter to estimate radioactive activity [19]. In the recent past, the idea of visualising radiation with detectors positioned closer to the imaged tissues has emerged [20]. Especially, some groups have been working on intraoperative imaging with [21] with fixed detectors attached to the bed paired with a movable PET laparoscope. Or directly with a freehand SPECT system [22] and drop-in gamma probes [23].

Recently, much attention has been given to biointerfaced sensors, i.e. sensors that interface with biological tissues [24, 25]. Most of the research has been dedicated to fabricating on-skin sensors, commonly known as electronic-skin (E-Skin) [26–29]. In contrast, developing invasive sensors deployed on-organs is a trickier task, as there is a high risk to trigger an immune response [25]. However, this hazard can be leveraged by carefully designing them [25].

Although radiation can be detected directly using semiconductors [30], the preferred method is to intercalate a scintillating material between the source of the radiation and a photosensor [31]. Indeed, scintillators have a higher energy range, better sensitivity to lower-energy radiation and reduced cost in comparison with semiconductors [30].

What would be the potential benefits of integrating these concepts into radiation detectors that are directly attached to the organs? In the specific application of nuclear imaging, we hypothesise that bringing a

radiation detector closer to the source would improve the signal-to-noise ratio (SNR), thereby reducing the radiation dose required to obtain high-quality images [13, 20]. This would also extend the imaging while providing instantaneous feedback during surgery.

Therefore, we explore the concept of β particle visualisation using elastic detectors placed directly on the region of interest (ROI). We introduce a novel class of scintillation detectors deployed on-organs and pair them with commercial endoscopes to generate real-time visualisations of tumourous tissues within the target anatomy. The detectors must be sufficiently elastic to conform to the complex morphology of the organs and adapt to beating and breathing motions without irritating surrounding tissues. We refer to these detectors as *imaging skins* for the shared morphological and mechanical properties with their biological counterpart.

In section 2, we describe the materials requirements for developing stretchable radiation detectors that can produce functional intraoperative images. Section 3 explores the concept of imaging skins, focusing on their deployment and integration into the surgical workflow to enable real-time imaging of tumours during RGS. The imaging skins, in their essence, must be capable of transducing radiation into a visible output. Consequently, we discussed the limitations and challenges associated with integrating these devices into clinical practice in relevant sections of the manuscript.

2. Radiation detection and image reconstruction

2.1. Beta-emitters

In clinical settings, β-radiation have energies in the ∼100–1000 keV range [37], as reported in table 1. It is important to note that many radioisotopes are tuned for PET imaging, thus catching positron (β_+)/electron annihilation. The direct detection of beta radiation is less common, but the imaging can be recommended when radiopharmaceuticals uptaking organs are close to the surgical site, as in the case of the uptake of ^{18}F-FDG in the brain, kidneys and bladder [38].

2.1.1. Positive beta decay (positron β_+)

When a beta-positive radiotracer decays, it releases a positron. This particle can only travel a short distance (∼1 mm) [34] before its annihilation upon interaction with an electron. The currently available radioprobes focus on detecting the positron energy before it encounters an electron by using inorganic scintillating material such as CsI:Tl [39]. Nonetheless, the radiopharmaceuticals can accumulate in distant organs, creating background noise due to the 511 keV γ-rays detection. Many methods can help isolate this radiation signal, such as gamma subtraction. Though, it implies including a means to detect γ and β_+ radiation simultaneously.

2.1.2. Negative beta decay (electron β_-)

Another solution, the detector must be designed to only catch β_--radiation- electron of a few MeV [19, 37]. β_-—imaging does not suffer from background noise due to tracer uptake in surrounding healthy tissues since electrons can only travel a few millimetres in water and tissues [37]. As a result, these radiations can only be detected through direct contact [40]. With the direct detection of beta radiation in RGS, we could minimise the amount of radioactive tracer injected. Hence, we would reduce the overall radiation dose received by the patient and the medical team. Moreover, this absence of signal contamination from background organs allows small tumours to be detected [41].

Regardless, β_- radiation is still secondary in diagnostic imaging and the quantity of radiopharmaceuticals is reduced. Yet, commonly used isotopes such as ^{90}Y or ^{131}I emit them. We referred the reader to the table 1 for commonly used β-emitting radioisotopes.

2.2. Scintillator requirements

Selecting the appropriate scintillator to target a specific radiation type while ensuring reasonable costs for a single-use medical device is a challenging task. This article highlights key features to seek when selecting suitable light-emitting agents for their application in imaging skins. Although traditional scintillators were initially based on inorganic materials, their toxicity and high production costs may limit their use in intraoperative applications. However, the field of scintillation has expanded greatly and offers many new possibilities, an advantage that we delve into in this article [42, 43].

New scintillators must meet the current standards in medical imaging, need to be easily embedded in stretchable materials and be able to convert radiation into optical information with a high light output. Based on the work of [42, 44, 45], we outline the essential characteristics for a scintillator to achieve valuable

Table 1. Most common beta-emitters in tumour imaging. Adapted from Richter *et al* [32], Conti and Eriksson [33], Lau *et al* [34], Kumar and Ghosh [35] and Crisan *et al* [36].

			β Emission energy (keV)	
	Isotopes	Half-life	Mean	**Max**
β^+	^{11}C	20.4 min	386	960
	^{18}F	1.8 h	250	635
	^{64}Cu	12.7 h	278	653
	^{68}Ga	1.2 h	836	1899
	^{89}Zr	3.3 days	396	902
	^{124}I	4.18 days	687 975	1535 2138
β^-	^{64}Cu	12.8 h	579	
	^{90}Y	64.24 h	2280	
	^{131}I	8.02 days	606	

Table 2. Key criteria for selecting optimal scintillators [45].

Characteristic	Criteria
Light yield	$>20\,000$ photons MeV^{-1}
Stopping power	100% at 2 mm
Decay	$<10\,\mu$s
Afterglow	$<0.1\%$ @ 3 ms
Thermal stability	$\pm 0,1\%$ per °C
Spectrum	500–700 nm

output and summarise them in table 2. In the following paragraph, we review these specifications and expand them to meet our specific needs.

- **Emission peak (nm)** In this article, we explore the idea of detecting the light emitted by scintillating stretchable detectors with commercially available endoscopic cameras, such as the couple-charge device recently proposed in [46] based on Cherenkov luminescence imaging. Therefore, since these detectors are designed to image photons in the visible spectrum, the peak emission of the scintillating material must be in the same range. For instance, the peak photo-response of silicon photodetectors is 400–900 nm [45], and the maximum sensitivity region of CMOS and CCD cameras is around 500–700 nm [47].
- **Light yield (photons MeV^{-1})** The light yield of a scintillating material is its tendency to generate light according to the absorbed particle energy. This parameter is critical when multiple sources of radiation can impact the detector. Particularly this could help discern particles with different specific energy such as 511 keV gamma radiation from beta particles with a few MeV [42].
- **Density (g cm^{-3}) and atomic number** With high density and a large atomic number, we ensure that all the particles that reach the detector will produce scintillation and not only go through the material. Furthermore, this can help reduce the depth of material required, which is essential to obtain stretchable imaging skins [42].
- **Decay time (s)** To monitor these imaging skins in real-time, we need a detector with a fast decay. In modern CT scanners, the refreshing rate is higher than 10 kHz [44]. However, commercial cameras have a short exposure time. The averaged shutter speed is in the ms range (100 Hz), but scientific cameras commonly achieve a 1 kHz refreshing rate [47]. Therefore, Lecoq suggests that the scintillator decay duration should be as short as possible and at least shorter than 10 μs [44].
- **Afterglow (%)** Ideally, the scintillator should not express any afterglow as it will add noise to the image. A scintillator with an afterglow smaller than 0.1% after 3 ms is considered sufficient [44].
- **Raw material price** Ideally, the cost of the raw material and its fabrication price must be minimal. For instance, Lutetium (Lu) composed scintillators, such as (LuI3: Ce3+), meet many of these criteria, as reported in 3, but their fabrication cost makes it a hindrance to their application in clinics [42].
- **Stability** The quality and efficiency of the scintillator should not be affected by external factors such as temperature, radiation, mechanical manipulation or time. For instance, we expect to employ these imaging

skins on the surface of organs or the bare skin of the patient. Therefore, the scintillator must prove stability between room and body temperature (20 °C–37 °C) [42].

- **Biocompatibility** Conventional scintillators made of inorganic materials have historically been employed in medical imaging for their high light output [42]. However, they are usually composed of toxic metal elements such as lead, which is a significant obstacle to their translation in surgery [42]. Organic scintillators were investigated for many decades [48], but their weak light yield limited their application in medical imaging [49].

  Nonetheless, these molecules are more easily manipulable and therefore deposited with low-cost techniques at room temperature [50]. Recently, some organic scintillators showed similar or even better light yield than some common scintillators [50, 51], as reported in table 3. Wang *et al* even developed a method to enhance the radioluminescence of metal-free organic scintillators [51].

Several groups have recently developed scintillators specifically for flexible imaging [46, 52, 53]. In this perspective article, we aim to explore and push the concept further with elastic scintillators designed for surgical imaging. Although creating such images is feasible, identifying suitable materials is crucial. In the following section, we discuss materials able to facilitate soft intraoperative imaging.

2.3. Substrate

Intraoperative stretchable detectors must comply with strict specifications to enable their use in clinical practice, especially when it comes to surgical applications. The most important aspect is biocompatibility—which prevents body rejection and inflammation at the imaging skin deployment site. Multiple research groups investigated these needs [56–59]. We summarised them in the following section and expanded this list with our identified requirements. Finally, we regrouped potential materials in table 4.

2.3.1. Biocompatibility

Implanted devices must meet the requirements defined by ISO 10993 [60]. The material should not trigger an immune response from irritation or noncompliance with the surrounding tissues. It should be hemocompatible, not cytotoxic, and minimise biofouling [59, 60].

2.3.2. Biodegradability

The material used to make the imaging skins must be biodegradable: any degradation should not create secondary infections. If any deterioration of dust should happen in the body, the human body must be capable of disposing of it by phagocytosis, bioabsorption, or metabolisation [58]. Finally, any non-biodegradable material must be well encapsulated.

2.3.3. Stretchability

The stretchability of a specific material ensures that the imaging interface can adapt to complex tissue anatomies and deformations induced by natural motion such as breathing or heartbeats [59]. The stretchability is a measure of the tensile strength, the maximum stress a material can endure before deforming or breaking [61]. The stretchability can be intrinsic [62] or engineered, by integrating serpentine architectures in non-stretchable materials for instance [57].

A morphological mismatch between medical devices and soft tissues can create a gap between the entities. This can lead to irritation of the tissues from the repeated friction and can trigger immune responses [59]. Therefore, different research groups agree on the fact that mechanical conformability is essential to biocompatibility [63]. The inflammatory response is minimised when the imaging skin-like sensor has Young's modulus that matches the modulus of tissue [59]. Specifically, the elastic modulus of human tissue ranges from only a few kPa (for the brain tissues) [64] to a few GPa with bones [63], as illustrated in figure 2. Moreover, displacement of the imaging sensor will result in performance degradation and additional noise. Therefore, the material selected to create imaging skin systems must be adequate for the specific type of tissue targeted within the human body.

2.3.4. Optical properties

For this application, the material must have suitable transparency. Indeed, the material must not attenuate the light signal generated and therefore be transparent to impede light dispersion. High nanoparticle concentration can also cause this phenomenon. For instance, in [66], the detector transmittance ranges from 65% to 85% according to the filler concentrations.

Table 3. Overview of scintillators properties. Data extracted from [43, 44, 50, 54, 55]. Favourable characteristics were highlighted in bold. In the heading, the density (ρ), effective atomic number (Z_{eff}), emission wavelength (λ), and primary scintillation decay time (τ) are represented by the corresponding abbreviations.

	Formula	Scintillator family	ρ (g cm^{-3})	Z_{eff}	Light yield (ph MeV^{-1})	τ (ns)	Afterglow (%)	λ (nm)
Inorganic	BGO	Traditional	**7.13**	**75.2**	8200	300	—	505
	NaI:Tl	Traditional	3.67	**50.8**	**43 000**	230	—	415
	CsI:Tl	Traditional	4.51	**54**	**66 000**	1000	2 @3 ms	560
	LSO	Traditional	**7.4**	11.4	**27 000**	**40**	—	420
	CsPbBr3	Pb-halide perovskite	—	—	**21 000**	**8.09**	—	525
	$Cs_3Cu_2I_5$:Tl^+	Doped Pb-free perovskite	—	—	**87 000**	957/717	0.17 @10 ms	440–510
Organic	Anthracene	Organic crystals	1.28	5.24	16 000	**30**	0.001 @1 μs	447
	Stilbene	Organic crystals	1.16	5.14	8000	**4.5**	—	410
	Naphthalene	Organic crystals	0.96	5.18	2000	**80**	—	348
	p-Terphenyl	Liquid solution	—	—	9200	**5**	—	440
	4CzTPN-Bu	Thermally Activated Delayed Fluorescence	—	—	**44 900**	**10.9**	0.01 @1 μs	555
	DMAc-TRZ	Thermally Activated Delayed Fluorescence	1.19	—	**73 500**	**20**	0.1 @1 μs	630
Hybrid	LuI_3:Ce^{3+}	Ce^{3+}-doped inorganic	5.7	**60.5**	**98 000**	**33**	—	475
	$(C_{38}H_{34}P_2)MnBr_4$	Organic manganese halide	1.65	4	**80 000**	3.18×10^5	—	517
	$C_{10}H_{22}BrCuIN$	Organic-Inorganic halide	1.94	8	**25 000**	2230	—	464

Table 4. Substrate materials and properties. Reproduced from [56]. CC BY 4.0.

Material	Material composition	Young's modulus (Pa)	Stretchability (%)	Biocompatible/ Biodegradable	Transparency
Silicone elastomer (Ecoflex00-30)	Organic	0.07 MPa	900%	Y/N	Translucent
Silicone elastomer (Sylgard184)	Organic	1.32–2.97 MPa	120%	Y/N	Yes
Silicone elastomer (Silbione LSR4330)	Organic	1.38 MPa	750%	Y/N	Yes
Parylene (VSI Parylene C)	Organic	2800 MPa	200%	Y/N	Yes
Polyethylene terephthalate (PET)	Organic	230 MPa	120%	Y/N	Yes (amorphous)
Polycaprolactone (PCL)	Organic	340.2 MPa	853.8%	Y/Y	No
Polyimide (PI)	Organic	280MPa	80%	Y/N	No
Polyethylenenaphthalate (PEN)	Organic	280 MPa	90%	Y/N	84% @0.075 mm
Polyethersulfone (PES)	Organic	2654.5 MPa	100%	Y/N	Yes
Polytetrafluoroethylene (PTFE)	Organic	0.0 6 MPa	400%	Y/N	Yes
Poly(lactic-co-glycolic acid) (PLGA)	Organic	2000 MPa	3%–10%	Y/Y	No
Cyclicole fin polymer (Zeonor1020R)	Organic	2100 MPa	90%	Y/N	Yes—92% @3 mm
Silk fibroin (dry)	Organic	2500 MPa	2.1%	Y/Y	Yes
Silk fibroin (wet)	Organic	16.7 Mpa	127.8%	Y/Y	Yes

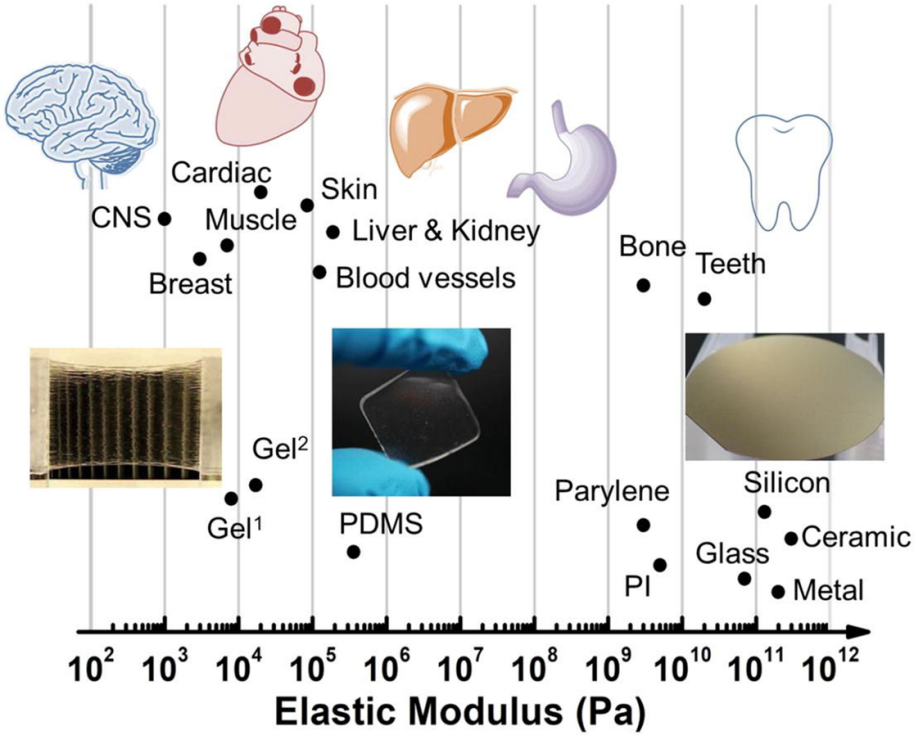

Figure 2. Elastic moduli comparison between human tissue, organs and diverse material. The elastic modulus of human tissue ranges from only a few kPa (for the brain tissues) [64] to a few GPa with bones [63]. Matching the substrate and image tissue moduli can help facilitate imaging and ensure a minimising inflammatory response. Reprinted from [65], Copyright (2019), with permission from Elsevier.

2.3.5. Structural design

Although the design of the scintillator is not directly related to the material characteristics. We think that it is an important feature that must be carefully selected. Indeed, the shape of the device directly affects its biocompatibility, altering the distribution of forces at the tissue-sensor interface [25].

For instance, controlling the detector thickness is crucial. By reducing the detector thickness, conformability and resolution can be improved by lowering the number of beta particles interacting with the substrate rather than the scintillator. However, this also increases the likelihood of radiation not interacting with the scintillating materials and remaining undetected [45, 52]. Hence, while the scintillator thickness should be minimised to ensure ease of deployment and adaptability to the surgical environment, the absorption of a sufficient amount of radiation to obtain suitable SNR should be always guaranteed.

Furthermore, selecting the optimal thickness depends on other factors, including the radioisotopes being detected and their energy range, as well as how they interact with the substrate. For instance, determining the minimum thickness to capture radiation requires consideration of factors such as the type of particles being detected and potential interference from annihilation gamma rays. Therefore, selecting an appropriate thickness is a delicate balancing act that involves considering all these parameters. To facilitate this, an automated platform for parameter testing in simulation could be developed.

2.4. State-of-the art in stretchable scintillators

To date, only one flexible scintillator has been used clinically to detect β_+ emissions. In [52], the authors evaluated the performance of their scintillator for autoradiography with a radiation-shielded EMCCD camera. Though they did not disclose the specifications of their material, they were able to detect activity at 0.9 kBq ml^{-1} for ^{18}F using a 6 μm flexible scintillator. In [67], a 12 μm thick version of the scintillator was used to detect tumour margins in breast-conservation surgery (BCS). They successfully proved that their technique was efficient for the intraoperative assessment of excised surgical specimens.

The scintillator could not conform to the specimen shape, possibly due to the limited stretchability of the selected material. Also, using ^{18}F radiopharmaceutical agents for breast cancer imaging is a suboptimal solution, and increasing the injected dose improves imaging sensitivity. Hence, it is crucial to establish a reference that correlates radiation dose to the pathologies. In summary, this study confirms the potential of scintillators for detecting beta particles in clinical settings. However, further research is necessary to achieve this goal.

In both applications, there is a clear advantage—every time the flexible scintillator was employed, the acquisition duration was significantly reduced. In [52], it took 300 s in comparison to micro-PET/CT which took 30–35 min by image acquisition time. In [46] the acquisition time was about 10 s, in comparison with 180–300 s with Cherenkov luminescence imaging. In these papers, the authors used commercially available scintillators. Although this simplifies the development of their protocol, looking at a new scintillator could be greatly beneficial, as acknowledged by the authors in [46].

Other groups have demonstrated the potential of flexible and/or stretchable radiation detectors but focused on catching x-rays. Despite the different energy ranges of beta particles and x-rays, the mechanism of scintillation is comparable. This is because scintillation converts energy from incoming radiation into light. Thus, we can apply some of their findings to the detection of beta particles.

Oliveira *et al* demonstrated the integration of scintillators into stretchable materials that can conform to human organs and perform high-quality imaging. The sensor is made of a safe polymer material for biomedical applications [66], and performed comparably to commercially available sensors. In their study [68], Ou *et al* developed a high-resolution, three-dimensional x-ray imaging method that does not require flat-panel detectors, by using a series of solution-processable, lanthanide-doped nano-scintillators with ultralong-lived x-ray trapping. While thin-film transistor detectors offer great sensitivity, they are expensive and have limited resolution [68].

Xu *et al* also fabricated a stretchable scintillator that is made of organic manganese halide powders mixed with polydimethylsiloxane [54]. Similarly, Mao *et al* developed a stretchable scintillator by blending organic manganese halide powders with polydimethylsiloxane, which serves as an organic-inorganic cuprous halide sensor [55]. Their scintillator demonstrates nearly all expected characteristics. They also proved that the scintillator can be fabricated inexpensively and integrated within a system, while also showing remarkable stability to bending and to the environment with emission peaks slightly outside our range. Nonetheless, the authors successfully captured images of a small circuit chip, achieving a spatial resolution of 5.60 LP mm^{-1} and a light yield of 25 000 photons MeV^{-1}.

In the research presented here, the detectors were used *ex-vivo* through autoradiography [46, 52, 67]. However, employing a similar detection method during surgeries poses numerous challenges, particularly in MIS. Therefore, we discuss them in detail in the remainder of this article.

2.5. Data analysis

We previously explored materials suitable for producing stretchable scintillation detectors for intraoperative use. Ideally, the imaging skins should have a high spatial resolution (LP mm^{-1}) and meet the current standards for nuclear imaging. However, as seen in other imaging techniques, numerical analysis can further enhance this resolution. Moreover, simulating the radiation interaction with the imaging skin can help ensure the validity of the design consideration. Therefore, these medical devices would require a specific framework to obtain valuable medical images. In this article, we envision smaller and more affordable imaging systems that would surpass the capacity of conventional medical imaging devices. Therefore, in this section, we review how simulation and sensing could support the objective of stretchable imaging to acquire valuable medical images with commercially available cameras.

2.5.1. Simulation

Monte Carlo (MC) simulations are widely employed to model radiation transportation in different scientific fields [69]. Simulation of the interaction of radiation with human tissues can help improve the data analysis and image quality. Moreover, MC simulation can help model complex scenarios requiring large human, equipment and time resources [69, 70]. Plus, modelling the interaction between the radiation sources, human tissues and the imaging skins can help select the optimal design of these detectors. For instance, CT collimators were tailored to reduce scatter for multi-sliced detectors and CT. Simulation is a must for designing imaging skins [69]. In 2017, Roncali *et al* reviewed different applications of MC simulations for the design of radiation detectors and proposed unifying the simulation [70]. This approach could help select the materials while favouring the reconstruction of images. MC simulation could aid in modelling responses of specific organs, thus removing the need to adapt to the morphology of the patients [69].

2.5.2. Acquisition

To achieve our goal, we suggest utilising commercially available endoscopes to capture the light emitted by the radiation detectors. Indeed, endoscopes are by construction photodetectors already integrated into MIS. Nevertheless, we anticipate that the signal will be significantly influenced by the position of the endoscope relative to the scintillating skin. And further research will be crucial to ensure the high sensitivity of this system.

To avoid this issue, one solution would be to integrate the photodetector into the imaging skins. It would require using biocompatible stretchable photodetectors, which adds an extra layer of complexity and physical thickness to the radiation detectors. Moreover, incorporating the whole detection framework within the imaging skin would require developing a method to transfer sensor information.

Alternatively, CCD/CMOS sensors with a small or medium format are readily accessible in the market of mobile devices [71]. CCD/CMOS sensors have a maximum quantum efficiency of around 500–700 nm [47], an emission requirement that we want to match by carefully selecting the scintillator, as discussed in section 2.

2.5.3. Shape sensing

In the context of this work, there is a clear need to assess the methods to process the collated information, such as determining how topography can be related to the visual information and exploring ways to translate the data into meaningful medical images for clinicians. Integrating a method to detect the shape of the imaging skins is essential to obtain reliable and qualitative medical images.

Knowing the physical deformation of the imaging skins will help account for and correct signal discrepancies produced by the topography of the imaging skin and help improve the correctness of the images. The imaging skins will conform to the complex shape of internal organs. However, reconstructing or flattening images is a novel and ambitious challenge. In this paragraph, we explore different methods that could be employed to facilitate image reconstruction.

Numerous strategies have been derived to monitor the shape of surface 3D objects. Proprioceptive sensing can be contact-based—through the integration of physical sensors or non-contact-based through the detection or specific markers with cameras [72, 73].

Shape-sensing can also be performed through electrical resistance, impedance or capacitive strain sensing. It usually requires electrical circuits and complex wiring, which is inadequate for surgical settings [74]. Nonetheless, the miniaturisation of the data transceiver and the integration of the electrical circuit into the imaging skin could be a solution. Nonetheless, these sensing elements might impact radiation imaging with their metallic components. Lastly, shape-sensing has also been achieved using magnetism [75], although the sensing can be affected by local field distortion from other metallic objects in the field and might also affect the radiation imaging.

Ideally, shape sensing can be implemented by using visual sensing. Surgical robots already possess stereo imaging. Bai *et al* monitored the shape of an actuated soft surface with a displacement resolution of 0.006 ± 0.055 mm at 30 fps using a stereo camera and a 4×4 array of markers [72].

In [76], Zampokas *et al* worked on improving the method to perform 3D reconstruction from stereo-endoscopy. Using stereo-endoscopy can help the data analysis as it can help determine the image depth from the triangulation of matching pixels. However, the task is not as straightforward as it seems due to the precise resolution, shadowing or anything that could create visual occlusion and image distortion. Therefore, there are methods to automate this process and reconstruct the 3D images from this depth information.

Van Meerbeek *et al* showed how a cluster of optical fibres could help reconstruct the shape of a soft surface. They trained a machine learning algorithm to monitor the twisting and bending of an elastomer foam. Although their result is promising, their optoelectronic system is too bulky and thus inadequate for application in surgery [77]. Lun *et al* integrated a shape-sensing fibre optic, a fibre Bragg grating sensor (FBGS) in a spatial shape inside a silicon substrate [78]. Here, they also employed a neural network to reconstruct the shape and achieved an RMSE of 1.17 mm error. Similarly, McDonald-Bowyer *et al* incorporated an FBGS to track the deformation of a pneumatically-actuated silicon retractor during robotic-assisted laparoscopic surgery. Therefore providing means to correlate US images to the underlying organ morphology [79].

2.5.4. Image processing

Whilst large datasets of radiation imaging skins have yet to be obtained, such information sources could be a tool to help improve image processing. Deep learning had applications in many fields but especially proved useful in classification, denoising and improving image resolution [80]. Notably, it has already been used to improve CT imaging by helping remove ring artefact in CT scan [80].

In the proposed application, the scintillator must be as thin as possible to ensure stretchability for perfect coupling with the surface of the organ. However, it must be noted that the scintillator thickness impacts the quality of the image. A thicker scintillator will strengthen the signal but will induce a spatial blur. Therefore, spatial blur must be accounted for and corrected during image processing [81].

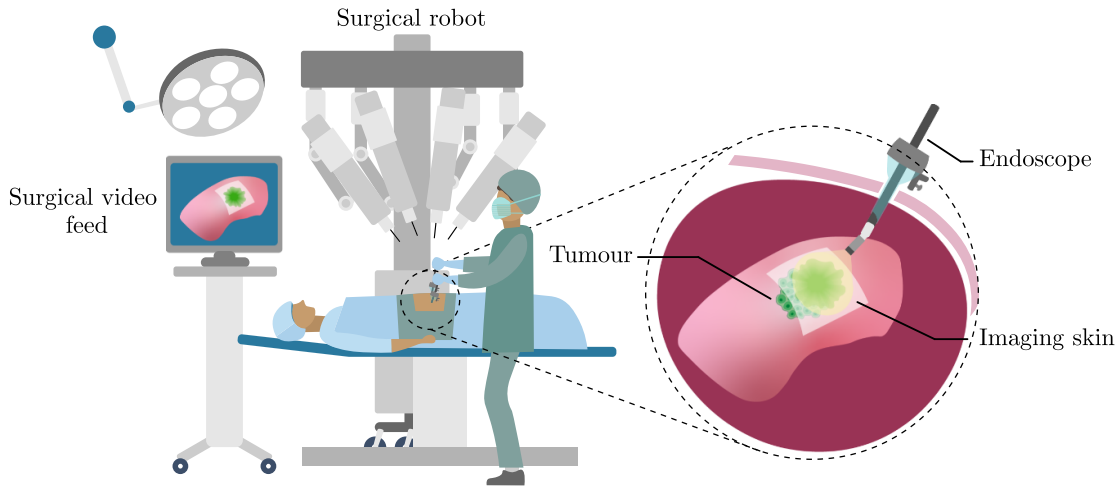

Figure 3. Illustration of the imaging concept. The imaging skin is deployed on the surface of an organ through a standard surgical port. It emits light revealing the underlying tumour structure. During the surgery, the clinician can visualise the endoscopic view stream on the screen.

3. Intraoperative use of the imaging skins

In this article, we introduce the concept of imaging skins. A novel beta-radiation detector that would be deployed laparoscopically on the surface of organs. As conventional nuclear imaging techniques such as PET or SPECT imaging, the imaging skins will be capable of transducing radiation activity into functional images. The imaging will rely on the scintillation capabilities of converting the energy by beta-particles into light. The scintillation of the imaging skin would then be recorded with a commercially available endoscope, as illustrated in figure 3. This is a main advantage compared to beta-probes on the market. Currently, they can only detect radiation over a small surface area. With imaging skins, monitoring larger tissue surfaces and overlaying the radiation signals over the endoscopic stream becomes possible. As of today, determining a PSM outcome takes days or weeks as it is done after the surgery. This extended and instantaneous information will help oncological surgeons make critical decisions. Especially, it will help them to discriminate tumour margins from healthy tissues in real-time during the surgery. In this section, we discussed the potential challenges of integrating imaging skins into a surgical workflow.

3.1. New surgical instruments

Surgical robot companies such as Intuitive Surgical offer a wide range of surgical tools [82]. In the foreseeable future, we can imagine that such companies will develop instruments specifically designed for manipulating thin deformable materials devices similar to imaging skins. These surgical tools will enable the insertion of the imaging skin through a trocar port and facilitate their swift and precise deployment on the ROI. Most importantly, the envisioned instruments should not damage the imaging skin nor the surrounding tissues during the surgery.

Manipulation of soft deformable objects is already a challenge in open inguinal hernia repair [83]. In this study, the authors demonstrated the effectiveness of rolling the mesh before the insertion to facilitate the deposition on the ROI. In MIS settings, rolling the imaging skins before the surgery would have a double beneficial impact. As mentioned, it would facilitate the placement of the imaging skin on the ROI. Secondly, it would also simplify the insertion through the trocar. It would also be possible to pre-pack the skin into a roll before surgery, making sure that the insertion through the trocar port remains easy while guaranteeing the sterility of the imaging skin, as illustrated in figure 4(a). Alternatively, we could envision having the imaging skin clipped by a laparoscopic gripper and rolled along the surgical tool during the insertion [83]. Similarly, [84] showed that the Swiss-roll (rolling with a thin layer of plastic between it) method facilitated the self-gripping mesh placement in laparoscopic surgery.

Another way to allow the insertion of the imaging skin would be to use an umbrella-like insertion method. For instance, in [85], they explore the deployment of a mesh using the umbrella technique. The idea is to clip the skin at the centre and push to insert it. One could envision an umbrella-like surgical tool designed to deploy deformable objects. The surgeon would load the skin before surgery, close the tool during insertion through the trocar and open it for deployment on the surgical site.

In the past decades, NASA has extensively explored the use of origami-based structures to the point that they organised a dedicated design competition on this topic [86]. However, origami-inspired techniques in surgery are currently at an early stage with solutions such as origami layer surgical retractor [87, 88]. Nonetheless, the challenge is similar. When in space, the goal is to fit a large solar panel into a rocket and deploy it in space. Here, the goal is to accommodate an imaging skin deployment system into a trocar port and deploy it onto the surgical site. In [89], Nakase *et al* investigated the insertion of large-sheet-style surgical material with an origami structure through a trocar. A solution that could fit the imaging skin insertion needs.

With an even more futuristic approach, a research group demonstrated the possibility of printing a hydrogel-based sensor directly on the surface of a breathing porcine lung [90]. Similarly, we could imagine printing the imaging skin with a surgery-safe material directly on the organ. Of course, the printing technology is still new and would have first to be minimised to fit through a trocar port.

3.2. Skin repositioning

Preoperative planning of skin placement is essential as the orientation of imaging skins affects image quality, as noted by King *et al* [46]. And as of yet, no studies have been conducted towards the automated positioning of stretchable scintillators [46]. Furthermore, unexpected events can occur during surgery. Therefore, integrating software that can instantly adapt to the actual environment and help reposition the imaging skins will be greatly beneficial.

For example, the initial placement may hinder the imaging of the entire ROI or novel information might be discovered during the surgery. Moreover, several images with various poses could be required to achieve adequate imaging. The entire process could even be repeated in different phases of the surgical procedure to ensure the complete resection of the tumour. However, positioning deformable objects in such an intricate environment is a complex task.

Looking at existing systems with potential for such application, in 2020 Morino *et al* proposed a gripper model to facilitate the task of picking and placing [91]. In [92], the graspers resemble human fingers in shape and in their capacity to provide proprioceptive force feedback through the BioTac finger.

Instead of a grasper, we could have a suctioning tool capable of lifting and moving the imaging skins, such as the flexible array called MISCA with liquid suction-control, as presented in [93]. Likewise, Stilli *et al* developed a pneumatic-actuated retractor to enhance the manipulation of organs during surgery without damaging the underlying tissues [94–96]. As mentioned, the imaging skin will have comparable material properties to the human tissues and could be employed similarly.

Bai *et al* presented a novel device almost in the realm of science fiction in the work presented in [72]. Instead of picking and placing the imaging skins with an external robot paired with an adapted surgical instrument, the imaging skins would be reprogrammable using electromagnetic actuation and visual feedback. With this idea in mind, we could externally control the skin, or more realistically, we could ensure that the skin would conform to the shape of the organ or fix any potential shadowing, therefore improving the imaging [72].

3.3. Camera positioning

Once the imaging skin is deployed, the camera needs to be accurately controlled to create images. Surgeons would need an optimum resolution to make accurate diagnoses and take the appropriate decisions. They must be able to see everything in the surgical field of view. However, they neither have the time nor the cognitive load to achieve that manually, and automatic or semi-automatic methods are preferred.

In 1988, Cowan and Kovesi studied the problem of automatic camera placement to improve the resolution of images of an object. They identify multiple constraints to validate the position of an imaging device, such as resolution, focus, field of view, visibility, view angle, and prohibited regions [97]. In this work, they computed a 3D space of all the camera positions to fully observe an object.

More recently, Ellis *et al* in the work presented in [98] developed a scientific interviewing strategy to develop autonomous camera control and help the surgeons focus on the surgical procedure during two different surgical tasks: suturing and knot tying. This research method could help understand what helps surgeons to visualise the entire surgical field and improve automatic camera positioning during automated robotic procedures.

These studies paved the way for the development of more advanced techniques for making camera positioning autonomous, yet these studies did not address camera alignment in the case of a light-emitting subject.

Staub *et al* worked on combining position-based and vision-based serving to bring the surgical instrument into the line of sight of the camera. They concluded that visual serving was mandatory to ensure perfect positioning of the surgical tool concerning optical markers [99]. Indeed, detecting visual markers on

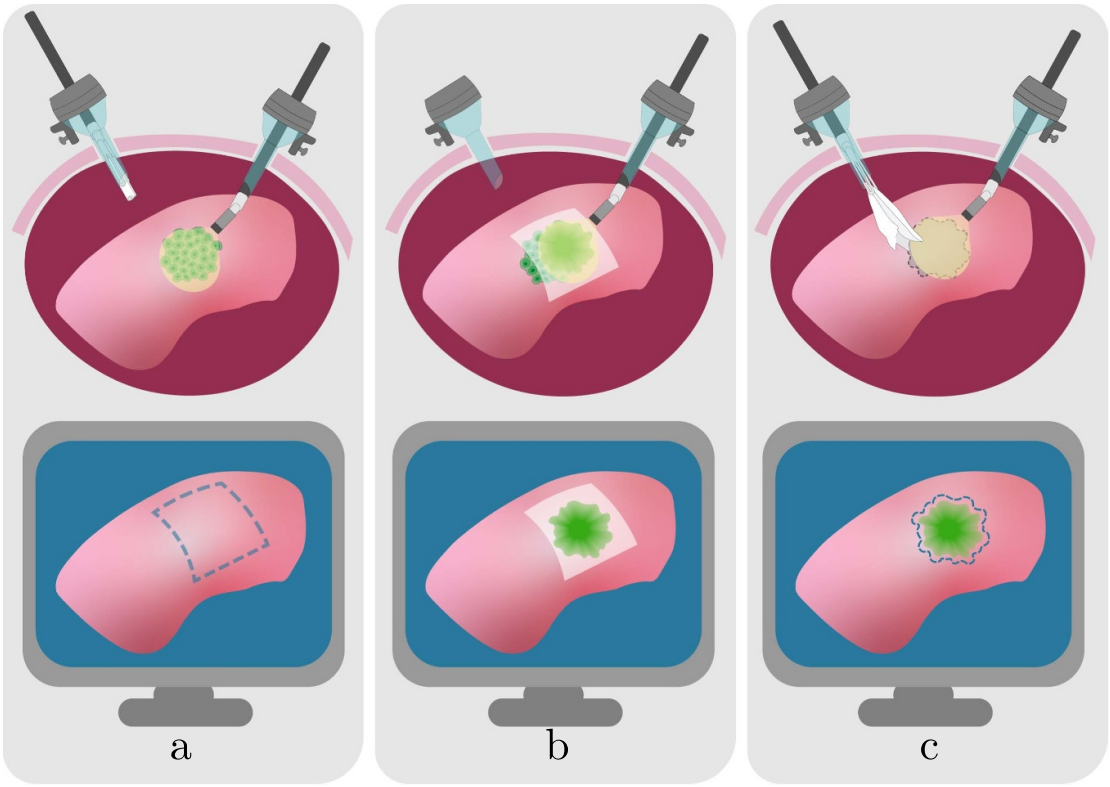

Figure 4. Top. Surgical field. Bottom. Corresponding surgical video feed, including superimposed augmented reality for each surgical step. (a) Insertion of the imaging skin into the surgical field through a trocar port. The software suggests imaging skin positioning from preoperative data and real-time endoscopic view. (b) Once the surgeon has deployed the imaging skin on-organ according to the previous suggestion, the scanning can start. (c) When the acquisition is over, the skin is removed, and the excision margin is overlayed on the real-time view.

the imaging skins could support positioning the camera. We can imagine incorporating visual landmarks in the centre of the imaging skin and edge detection. Although, it must be mentioned that it might be challenging to position the camera in such an enclosed space, and optimal positioning concerning these visual cues might be extremely demanding.

3.4. Data visualisation

In recent years, augmented reality (AR) has caught the interest of medical researchers [100–102]. In AR, the user can simultaneously visualise reality and any virtual shape or object. Therefore, any medical images could be superimposed in the surgical field to assist surgeons in decision-making.

For instance, during see-through AR, the surgeon will see the surrounding environment enhanced with computer-based projection via an interface such as the Microsoft Hololens 2 (MICROSOFT, Redmond, WA, US) or Samsung Gear VR (SAMSUNG, Seoul, South Korea). Mobile AR—integrating an external screen, such as a phone in the currently notorious game Pokemon Go—could also be a visualisation solution. Additionally, see-through AR could alleviate surgeon fatigue during laparoscopic procedures by eliminating the need for constant switching between medical images on a screen and direct observation of the surgical field [103].

Augmented reality can have dual applications with imaging skins. On the one hand, visual markers can help the surgeon and/or the surgical robot during the precise deposition of the sensor on the surface of an organ, as illustrated in figure 4(a). On the other hand, they can help register novel information to any preoperative images or help surgeons visualise the borders of the tumour during surgery, as depicted in figure 4(b).

As the study presented in [104] suggests, see-through AR can help surgeons visualise the structure of internal organs and decide on the best trocar placement. Likewise, superimposing preoperative images of the targeted tumour could help set an imaging skin quickly by visualising the expected tumour position. Peleka *et al* compared the state-of-the-art approaches to register MIS imaging information to preoperative 3D models of a patient's anatomy [105]. Although challenging, the techniques presented in this work seemed successful. Automating this task would ease surgeries and tremendously reduce the cognitive load of the surgeon, as the clinician would visualise the tumour directly and not integrate its position internally.

Besides, the user does not even need an interface and can directly see the projection of virtual objects into reality in spatial AR [100]. In clinical practice, the human or robotic placement of the skin could be looped with this visual feedback to match the location of the skin to these optical markers [104]. Moreover, it could facilitate 3D reconstruction of the underlying imaged structure by providing a precise template of multiple sensor poses [106].

Assuming perfect positioning of the imaging skins and the camera to obtain medical images of any underlying tumours: there is still the need to produce a rendering to help surgeons during excision. Nowadays, most medical images are computer-based, which eases the reading and enables post-processing analysis.

Once visualised with the imaging skin, the tumour edges could be projected onto the virtual image or directly on the organ's surface, using spatial AR, as depicted in figure 4(c). Additionally, AR can help with the continuous visualisation of the recorded data once the skin-like sensor is removed.

AR studies must guarantee that the quantity of information conveyed by the display will not affect the surgeon's attention. Moreover, the AR must have no latency and almost perfect alignment to the medical data to the patient organs [107].

4. Conclusions

This perspective offers the first insights into imaging skins, which are stretchable scintillators providing intraoperative feedback on tumour margins during surgical resections.

Out of the positive findings, we saw that state-of-the-art research in the related field proved that such detectors carry a sensitivity suitable for clinical translation [67]. Other research group demonstrated that the imaging skins could improve spatial resolution compared to a flat scintillator when conforming to the geometry of the specimen [46, 52]. Finally, the imaging skins can provide instantaneous feedback compared to the accepted methods of tumour margin assessment. And the radiation signal could be overlayed onto the endoscopic stream, providing continuous feedback to the surgeon during the excision.

To facilitate the task of researchers and engineers, we have discussed aspects which could lead to the successful development, deployment and clinical translation of bespoke imaging skins. Therefore, we reported on the β-emitting radiation sources available in clinical practice.

We identified a need to develop novel radiopharmaceuticals tuned to emit β_- particles. Indeed, all stretchable scintillators presented here used β_+ radiotracers such ^{18}F and ^{99m}Tc. Indeed, radiopharmaceuticals were standardised to PET and SPECT, but β_+ radiotracers represent a liability in this application as gamma-ray emission from positron–electron annihilation creates a background noise emanating from distant organs. β_- radiopharmaceuticals would not carry the same constraints. Additionally, using β_- would reduce the exposure to radiation of the medical team. And, the imaging skins could be the appropriate tool to enable intraoperative beta particle imaging.

Considering these radiation sources, we reviewed the materials required to fabricate the imaging skins. First, we focused on the scintillating molecules that can transduce radiation into visual information. Then, we explored surgery-compliant materials to embed these particles safely into stretchable imaging skins. In both cases, we listed the ideal requirements to attain our objectives. It should be noted that repeatability of the fabrication process is a must-have to ensure and provide reliable and comparable data.

Ideally, the deployment of the skins would be straightforward and not add to the—already significant—cognitive load of the surgeon. In practice, we know that adding a novel surgical task would extend the surgery duration. As discussed in section 3, we envision that fixing some degrees of freedom with the incorporation of robots and augmented-reality platforms would enhance human abilities and enable them to perform delicate manoeuvres that seemed out of reach in the past. Also, developing surgical instruments made to manipulate thin deformable devices would greatly help the surgical workflow.

Therefore, all the surgical steps must be discussed between engineers and clinicians to ensure the design of the most effective imaging protocol. Studies must be carried out to prove the usefulness of the imaging skin compared to state-of-the-art intraoperative tumour imaging protocols.

Afterwards, we focused on the data analysis. In this work, it was envisioned to use affordable cameras to record medical images. The algorithms that would treat this information are yet to be written. Namely, using stretchable materials with infinite degrees of freedom will not facilitate the task of engineers during image reconstruction. However, with simulation and integration of sensors, such as shape-sensing ones, they possess tools to accomplish the task. Moreover, the last generation computers have the computational capacities to process a large amount of data.

To summarise, there are many challenges to overcome before we see the imaging skins employed in surgery. Regardless, this emerging concept could revolutionise the intraoperative imaging field and lead to better outcomes for patients.

Data availability statement

No new data were created or analysed in this study.

ORCID iDs

S Dietsch https://orcid.org/0000-0002-0122-7210
L Lindenroth https://orcid.org/0000-0002-9108-4574
A Stilli https://orcid.org/0000-0002-4904-0500
D Stoyanov https://orcid.org/0000-0002-0980-3227

References

[1] Sullivan R *et al* 2015 Global cancer surgery: delivering safe, affordable and timely cancer surgery *Lancet Oncol.* **16** 1193–224
[2] Maloney B W, McClatchy D M, Pogue B W, Paulsen K D, Wells W A and Barth R J 2018 Review of methods for intraoperative margin detection for breast conserving surgery *J. Biomed. Opt.* **23** 1
[3] Voskuil F J, Vonk J, van der Vegt B, Kruijff S, Ntziachristos V, van der Zaag P J, Witjes M J H and van Dam G M 2021 Intraoperative imaging in pathology-assisted surgery *Nat. Biomed. Eng.* **6** 503–14
[4] Orosco R K *et al* 2018 Positive surgical margins in the 10 most common solid cancers *Sci. Rep.* **8** 1–9
[5] Shah P C, de Groot A, Cerfolio R, Huang W C, Huang K, Song C, Li Y, Kreaden U and Oh D S 2022 Impact of type of minimally invasive approach on open conversions across ten common procedures in different specialties *Surg. Endosc.* **36** 6067–75
[6] Clancy N T, Jones G, Maier-Hein L, Elson D S and Stoyanov D 2020 Surgical spectral imaging *Med. Image Anal.* **63** 101699
[7] Lauwerends L J *et al* 2021 Real-time fluorescence imaging in intraoperative decision making for cancer surgery *Lancet Oncol.* **22** e186–95
[8] Hu S, Kang H, Baek Y, El Fakhri G, Kuang A and Choi H S 2018 Real-time imaging of brain tumor for image-guided surgery *Adv. Healthcare Mater.* **7** 1800066
[9] Pradipta A R, Tanei T, Morimoto K, Shimazu K, Noguchi S and Tanaka K 2020 Emerging technologies for real-time intraoperative margin assessment in future breast-conserving surgery *Adv. Sci.* **7** 1901519
[10] Heidkamp J, Scholte M, Rosman C, Manohar S, Fütterer J J and Rovers M M 2021 Novel imaging techniques for intraoperative margin assessment in surgical oncology: a systematic review *Int. J. Cancer* **149** 635–45
[11] olde Heuvel J, de Wit-van der Veen B J, Huizing D M V, van der Poel H G, van Leeuwen P J, Bhairosing P A, Stokkel M P M and Slump C H 2021 State-of-the-art intraoperative imaging technologies for prostate margin assessment: a systematic review *Eur. Urol. Focus* **7** 733–41
[12] Li M, Liu H, Jiang A, Seneviratne L D, Dasgupta P, Althoefer K and Wurdemann H 2014 Intra-operative tumour localisation in robot-assisted minimally invasive surgery: a review *Proc. Inst. Mech. Eng.* H **228** 509–22
[13] Park H, Han K N, Choi B H, Yoon H, An H J, Lee J S and Kim H K 2022 Ultra-low-dose intraoperative x-ray imager for minimally invasive surgery: a pilot imaging study *Transl. Lung Cancer Res.* **11** 588–99
[14] Herrmann K, Nieweg O E and Povoski S P (eds) 2016 *Radioguided Surgery* (Cham: Springer International Publishing)
[15] Pashazadeh A and Friebe M 2020 Radioguided surgery: physical principles and an update on technological developments *Biomed. Tech.* **65** 1–10
[16] Selverstone B, Sweet W H and Robinson C V 1949 The clinical use of radioactive phosphorus in the surgery of brain tumors *Ann. Surg.* **130** 643–51
[17] Ge J, Zhang Q, Zeng J, Gu Z and Gao M 2020 Radiolabeling nanomaterials for multimodality imaging: new insights into nuclear medicine and cancer diagnosis *Biomaterials* **228** 119553
[18] Hoffman E J, Tornai M P, Janecek M, Patt B E and Iwanczyk J S 2004 Intraoperative probes and imaging probes *Emission Tomography: The Fundamentals of PET and SPECT* vol 26 (San Diego, CA: Academic) pp 335–58
[19] Thacker S C, Stack B C, Lowe V, Gaysinskiy V, Cool S, Nagarkar V V and Entine G 2008 A novel imaging beta probe for radioguided surgery *IEEE Nuclear Science Symp. Conf. Record* pp 3875–8
[20] Collamati F, Valdés Olmos R, Albanese A, Cocciolillo F, Di Giuda D and Collarino A 2022 Current use and potential role of radioguided surgery in brain tumours *Clin. Transl. Imaging* **10** 451–6
[21] Liyanaarachchi M, Shimazoe K, Takahashi H, Kobayashi E, Nakagawa K and Sakuma I 2020 Prototype detector for intraoperative PET-laparoscope system with a multi-layer movable detector *Nucl. Instrum. Methods Phys. Res.* A **958** 162788
[22] Bluemel C, Schnelzer A, Okur A, Ehlerding A, Paepke S, Scheidhauer K and Kiechle M 2013 Freehand SPECT for image-guided sentinel lymph node biopsy in breast cancer *Eur. J. Nucl. Med. Mol. Imaging* **40** 1656–61
[23] Abascal Junquera J M *et al* 2023 A drop-in gamma probe for minimally invasive sentinel lymph node dissection in prostate cancer *Clin. Nucl. Med.* **48** 213–20
[24] Hammock M L, Chortos A, Tee B C K, Tok J B H and Bao Z 2013 25th anniversary article: the evolution of electronic skin (E-Skin): a brief history, design considerations and recent progress *Adv. Mater.* **25** 5997–6038
[25] Zohar O, Khatib M, Omar R, Vishinkin R, Broza Y Y and Haick H 2021 Biointerfaced sensors for biodiagnostics *View* **2** 1–18
[26] Yang J C, Mun J, Kwon S Y, Park S, Bao Z and Park S 2019 Electronic skin: recent progress and future prospects for skin-attachable devices for health monitoring, robotics and prosthetics *Adv. Mater.* **31** 1904765
[27] Chen J, Zhu Y, Chang X, Pan D, Song G, Guo Z and Naik N 2021 Recent progress in essential functions of soft electronic skin *Adv. Funct. Mater.* **31** 2104686
[28] Cao H L and Cai S Q 2022 Recent advances in electronic skins: material progress and applications *Front. Bioeng. Biotechnol.* **10** 1–8
[29] Li W, Dong J, Zhang X and Fan F R 2023 Recent progress in advanced units of triboelectric electronic skin *Adv. Mater. Technol.* **8** 1–20
[30] Asuvaran A and Elatharasan G 2022 Design of two-dimensional photonic crystal-based biosensor for abnormal tissue analysis *Silicon* **14** 7203–10
[31] Hoheisel M 2006 Review of medical imaging with emphasis on x-ray detectors *Nucl. Instrum. Methods Phys. Res.* A **563** 215–24
[32] Richter J R, Kasten B B and Zinn K R 2016 *Imaging and Adenoviral Gene Therapy* 2nd edn (Amsterdam: Elsevier Inc.)

[33] Conti M and Eriksson L 2016 Physics of pure and non-pure positron emitters for PET: a review and a discussion *EJNMMI Phys.* **3** 8
[34] Lau J, Rousseau E, Kwon D, Lin K S, Bénard F and Chen X 2020 Insight into the development of PET radiopharmaceuticals for oncology *Cancers* **12** 1312
[35] Kumar K and Ghosh A 2021 Radiochemistry, production processes, labeling methods and immunopet imaging pharmaceuticals of iodine-124 *Molecules* **26** 414
[36] Crișan G, Moldovean-cioroianu N S, Timaru D G, Andrieș G, Ciuainap C, Chiș V, Căinap C and Chiș V 2022 Radiopharmaceuticals for PET and SPECT imaging: a literature review over the last decade *Int. J. Mol. Sci.* **23** 5023
[37] Gonzalez-Montoro A, Vera-Donoso C D, Konstantinou G, Sopena P, Martinez M, Ortiz J B, Carles M, Benlloch J M and Gonzalez A J 2022 Nuclear-medicine probes: where we are and where we are going *Med. Phys.* **49** 4372–90
[38] Franc B L, Mari C, Johnson D and Leong S P 2005 The role of a positron- and high-energy gamma photon probe in intraoperative localization of recurrent melanoma *Clin. Nucl. Med.* **30** 787–91
[39] Sabet H, Stack B C and Nagarkar V V 2015 A hand-held, intra-operative positron imaging probe for surgical applications *IEEE Trans. Nucl. Sci.* **62** 1927–34
[40] Mancini-Terracciano C *et al* 2019 Radio-guided surgery with β—radiation: tests on *ex-vivo* specimens *World Congress on Medical Physics and Biomedical Engineering 2018* (*IFMBE Proc.*) vol 68 (Singapore: Springer) pp 693–7
[41] Bertani E *et al* 2021 First *ex vivo* results of β—radioguided surgery in small intestine neuroendocrine tumors with 90 Y-DOTATOC *Cancer Biother. Radiopharm.* **36** 397–406
[42] Weber M J 2002 Inorganic scintillators: today and tomorrow *J. Lumin.* **100** 35–45
[43] Maddalena F *et al* 2019 Inorganic, organic and perovskite halides with nanotechnology for high-light yield x- and gamma-ray scintillators *Crystals* **9** 88
[44] Lecoq P 2016 Development of new scintillators for medical applications *Nucl. Instrum. Methods Phys. Res.* A **809** 130–9
[45] Lu L, Sun M, Wu T, Lu Q, Chen B and Huang B 2022 All-inorganic perovskite nanocrystals: next-generation scintillation materials for high-resolution x-ray imaging *Nanoscale Adv.* **4** 680–96
[46] King M T *et al* 2016 Flexible radioluminescence imaging for FDG-guided surgery *Med. Phys.* **43** 5298–306
[47] Thorlabs 2022 *sCMOS, CMOS, and CCD Cameras* (available at: www.thorlabs.com/images/Brochures/Thorlabs_ScientificCameras_Brochure.pdf)
[48] Sangster R C and Irvine J W 1956 Study of organic scintillators *J. Chem. Phys.* **24** 670–715
[49] Hajagos T J, Liu C, Cherepy N J and Pei Q 2018 High-Z sensitized plastic scintillators: a review *Adv. Mater.* **30** 1–13
[50] Ma W *et al* 2022 Thermally activated delayed fluorescence (TADF) organic molecules for efficient x-ray scintillation and imaging *Nat. Mater.* **21** 210–6
[51] Wang X *et al* 2021 Organic phosphors with bright triplet excitons for efficient X-ray-excited luminescence *Nat. Photon.* **15** 187–92
[52] Vyas K, Mertzanidou ThomyGrootendorst M, Tuch D S, Stoyanov D, Arridge S R and Macholl S 2018 Flexible scintillator autoradiography for tumor margin inspection using 18F-FDG *Proc. SPIE* **10478** 1047811
[53] Wang J X *et al* 2021 Medical applications of tissue-equivalent, organic-based flexible direct x-ray detectors *Nat. Photon.* **15** 187–92
[54] Xu L J, Lin X, He Q, Worku M and Ma B 2020 Highly efficient eco-friendly x-ray scintillators based on an organic manganese halide *Nat. Commun.* **11** 1–8
[55] Mao P, Tang Y, Wang B, Fan D and Wang Y 2022 Organic–inorganic hybrid cuprous halide scintillators for flexible x-ray imaging *ACS Appl. Mater. Interfaces* **14** 22295–301
[56] Herbert R, Kim J H, Kim Y S, Lee H M and Yeo W H 2018 Soft material-enabled, flexible hybrid electronics for medicine, healthcare and human-machine interfaces *Materials* **11** 187
[57] Liu K, Tran H, Feig V R and Bao Z 2020 Biodegradable and stretchable polymeric materials for transient electronic devices *MRS Bull.* **45** 96–102
[58] Wang L, Jiang K and Shen G 2021 Wearable, implantable and interventional medical devices based on smart electronic skins *Adv. Mater. Technol.* **6** 2100107
[59] Chitrakar C, Hedrick E, Adegoke L and Ecker M 2022 Flexible and stretchable bioelectronics *Materials* **15** 1664
[60] ISO 10993-1:2018(en) 2018 *Biological Evaluation of Medical Devices—Part 1: Evaluation and Testing Within a Risk Management Process* (International Organisation for Standardization) (available at: www.iso.org/obp/ui#iso:std:iso:10993:-1:ed-5:v2:en)
[61] Fan X, Nie W, Tsai H, Wang N, Huang H, Cheng Y, Wen R, Ma L, Yan F and Xia Y 2019 PEDOT:PSS for flexible and stretchable electronics: modifications, strategies and applications *Adv. Sci.* **6** 1900813
[62] Trung T Q and Lee N E 2017 Recent progress on stretchable electronic devices with intrinsically stretchable components *Adv. Mater.* **29** 1603167
[63] Bettinger C J 2018 Recent advances in materials and flexible electronics for peripheral nerve interfaces *Bioelectron. Med.* **4** 1–10
[64] Fallenstein G T, Hulce V D and Melvin J W 1969 Dynamic mechanical properties of human brain tissue *J. Biomech.* **2** 217–26
[65] Wu X and Peng H 2019 Polymer-based flexible bioelectronics *Sci. Bull.* **64** 634–40
[66] Oliveira J, Correia V, Costa P, Francesko A, Rocha G and Lanceros-Mendez S 2018 Stretchable scintillator composites for indirect x-ray detectors *Composites* B **133** 226–31
[67] Jurrius P A G T *et al* 2021 Intraoperative [^{18}F]FDG flexible autoradiography for tumour margin assessment in breast-conserving surgery: a first-in-human multicentre feasibility study *EJNMMI Res.* **11** 28
[68] Ou X *et al* 2021 High-resolution X-ray luminescence extension imaging *Nature* **590** 410–5
[69] Zaidi H and Ay M R 2007 Current status and new horizons in Monte Carlo simulation of X-ray CT scanners *Med. Biol. Eng. Comput.* **45** 809–17
[70] Roncali E, Mosleh-Shirazi M A and Badano A 2017 Modelling the transport of optical photons in scintillation detectors for diagnostic and radiotherapy imaging *Phys. Med. Biol.* **62** R207–35
[71] Mostovych N A *et al* 2018 Digital image capture for high-resolution medical x-ray diagnostics *Proc. SPIE* **10763** 107630E
[72] Bai Y *et al* 2021 A dynamically reprogrammable metasurface with self-evolving shape morphing *Nature* **609** 701
[73] Shaik R A and Rufus E 2021 Recent trends and role of large area flexible electronics in shape sensing application—a review *Ind. Robot.* **48** 745–62
[74] Jauhiainen J, Pour-Ghaz M, Valkonen T and Seppänen A 2021 Nonplanar sensing skins for structural health monitoring based on electrical resistance tomography *Comput.-Aided Civil Infrastruct. Eng.* **36** 1488–507
[75] Hermanis A, Cacurs R and Greitans M 2016 Acceleration and magnetic sensor network for shape sensing *IEEE Sens. J.* **16** 1271–80
[76] Zampokas G, Tsiolis K, Peleka G, Mariolis I, Malasiotis S and Tzovaras D 2018 Real-time 3d reconstruction in minimally invasive surgery with quasi-dense matching *IST 2018—IEEE Int. Conf. on Imaging Systems and Techniques, Proc.*

[77] Van Meerbeek I M, De Sa C M and Shepherd R F 2018 Soft optoelectronic sensory foams with proprioception *Sci. Robot.* **3** 1–8
[78] Lun T L T, Wang K, Ho J D L, Lee K H, Sze K Y and Kwok K W 2019 Real-time surface shape sensing for soft and flexible structures using fiber Bragg gratings *IEEE Robot. Autom. Lett.* **4** 1454–61
[79] McDonald-Bowyer A, Dietsch S, Dimitrakakis E, Coote J M, Lindenroth L, Stoyanov D and Stilli A 2023 Organ curvature sensing using pneumatically attachable flexible rails in robotic-assisted laparoscopic surgery *Front. Robot. AI* **9** 1–14
[80] Yuan L, Xu Q, Liu B, Wang Z, Liu S, Wei C and Wei L 2021 A deep learning-based ring artifact correction method for x-ray CT *Radiat. Detect. Technol. Methods* **5** 493–503
[81] Adams J *et al* 2021 An approach to characterizing spatial aspects of image system blur *Stat. Anal. Data Mining* **14** 583–95
[82] Intuitive Surgical 2023 Da vinci X/Xi system instrument and accessory catalog pp 1–26 (available at: www.intuitive.com/en-us/-/media/ISI/Intuitive/Pdf/xi-x-ina-catalog-no-pricing-us-1052082.pdf)
[83] Lechner M N, Jäger T, Buchner S, Köhler G, Öfner D and Mayer F 2016 Rail or roll: a new, convenient and safe way to position self-gripping meshes in open inguinal hernia repair *Hernia* **20** 417–22
[84] Zhu X, Liu J, Wei N, Liu Z and Tang R 2020 A study of the "Swiss-roll" folding method for placement of self-gripping mesh in TAPP *Minim. Invasive Ther. Allied Technol.* **31** 1–7
[85] Durai R, Mownah A and Ng P C H 2010 Umbrella and roll-up techniques of mesh insertion for laparoscopic hernia repair: a comparative study *Surg. Endosc.* **24** 949–51
[86] Schlieder S 2022 *Ultralight Starshade Structural Design—NASA* (available at: www.nasa.gov/ultralight-starshade-structural-design-challenge)
[87] Banerjee H, Li T K, Ponraj G, Kirthika S K, Lim C M and Ren H 2020 Origami-layer-jamming deployable surgical retractor with variable stiffness and tactile sensing *J. Mech. Robot.* **12** 1–10
[88] Meloni M, Cai J, Zhang Q, Sang-Hoon Lee D, Li M, Ma R, Parashkevov T E and Feng J 2021 Engineering origami: a comprehensive review of recent applications, design methods and tools *Adv. Sci.* **8** 1–31
[89] Nakase Y, Nakamura K, Sougawa A, Nagata T, Mochizuki S, Kitai S and Inaba S 2017 A novel procedure for introducing large sheet-type surgical material with a self-expanding origami structure using a slim trocar (chevron pleats procedure) *Surg. Endosc.* **31** 3749–54
[90] Zhu Z, Park H S and McAlpine M C 2020 3D printed deformable sensors *Sci. Adv.* **6** 1–11
[91] Morino K, Kikuchi S, Chikagawa S, Izumi M and Watanabe T 2020 Sheet-based gripper featuring passive pull-in functionality for bin picking and for picking up thin flexible objects *IEEE Robot. Autom. Lett.* **5** 2007–14
[92] Zheng Y, Veiga F F, Peters J and Santos V J 2022 Autonomous learning of page flipping movements via tactile feedback *IEEE Trans. Robot.* **38** 2734–49
[93] Nishita S and Onoe H 2017 Liquid-filled flexible micro suction-controller array for enhanced robotic object manipulation *J. Microelectromech. Syst.* **26** 366–75
[94] Stilli A, Dimitrakakis E, D'ettorre C, Tran M and Stoyanov D 2019 Pneumatically attachable flexible rails for track-guided ultrasound scanning in robotic-assisted partial nephrectomy—a preliminary design study *IEEE Robot. Autom. Lett.* **4** 1208–15
[95] Ettorre C D, Stilli A, Dwyer G, Neves J B, Tran M and Stoyanov D 2019 Semi-autonomous interventional manipulation using pneumatically attachable flexible rails *IEEE Int. Conf. on Intelligent Robots and Systems* pp 1347–54
[96] Wang C, Komninos C, Andersen S, D'Ettorre C, Dwyer G, Maneas E, Edwards P, Desjardins A, Stilli A and Stoyanov D 2020 Ultrasound 3D reconstruction of malignant masses in robotic-assisted partial nephrectomy using the PAF rail system: a comparison study *Int. J. Comput. Assist. Radiol. Surg.* **15** 1147–55
[97] Cowan C K and Kovesi P D 1988 Automatic sensor placement from vision task requirements *IEEE Trans. Pattern Anal. Mach. Intell.* **10** 407–16
[98] Ellis R D, Munaco A J, Reisner L A, Klein M D, Composto A M, Pandya A K and King B W 2016 Task analysis of laparoscopic camera control schemes *Int. J. Comput. Assist. Radiol. Surg.* **12** 576–84
[99] Staub C, Knoll A, Osa T and Bauernschmitt R 2010 Autonomous high precision positioning of surgical instruments in robot-assisted minimally invasive surgery under visual guidance *6th Int. Conf. on Autonomic and Autonomous Systems (ICAS 2010)* pp 64–69
[100] Makhataeva Z and Varol H A 2020 Augmented reality for robotics: a review *Robotics* **9** 21
[101] Edwards P J E, Chand M, Birlo M and Stoyanov D 2021 The challenge of augmented reality in surgery *Digital Surgery* (Cham: Springer) pp 121–35
[102] Birlo M, Edwards P J, Clarkson M and Stoyanov D 2022 Utility of optical see-through head mounted displays in augmented reality-assisted surgery: a systematic review *Med. Image Anal.* **77** 102361
[103] Zorzal E R, Campos Gomes J M, Sousa M, Belchior P, da Silva P G, Figueiredo N, Lopes D S and Jorge J 2020 Laparoscopy with augmented reality adaptations *J. Biomed. Inform.* **107** 103463
[104] Mahmoud N, Grasa G, Nicolau S A, Doignon C, Soler L, Marescaux J and Montiel J M M 2017 On-patient see-through augmented reality based on visual SLAM *Int. J. Comput. Assist. Radiol. Surg.* **12** 1–11
[105] Peleka G, Zampokas G, Mariolis I, Malasiotis S and Tzovaras D 2018 Intra-operative 3D registration of MIS reconstructed surfaces to pre-operative models *IST 2018—IEEE Int. Conf. on Imaging Systems and Techniques, Proc.* pp 1–6
[106] Mahvash M and Tabrizi L B 2013 A novel augmented reality system of image projection for image-guided neurosurgery *Acta Neurochir.* **155** 943–7
[107] Desselle M R, Brown R A, James A R, Midwinter M J, Powell S K and Woodruff M A 2020 Augmented and virtual reality in surgery *Comput. Sci. Eng.* **22** 18–26